J Mater Sci: Mater Electron **(2025) 36:866**

Development of expanded graphite composite-based triboelectric nanogenerator for sustainable energy generation

Sebghatullah Amini[1], Rumana Farheen Sagade Muktar Ahmed[1], Sangamesha Madanahalli Ankanathappa[2], and Krishnaveni Sannathammegowda[1,*]

[1] *Department of Studies in Physics, University of Mysore, Mysuru, Karnataka 570006, India*
[2] *Department of Chemistry, The National Institute of Engineering, Mysuru, Karnataka 570008, India*

Received: 5 January 2025
Accepted: 11 May 2025
Published online: 24 May 2025

ABSTRACT

Triboelectric Nanogenerators (TENG), transformational devices that harness mechanical energy to generate electricity, are pivotal for driving the advancement of autonomous technologies in today's mobile-centric world. In this study, a TENG is developed, using a novel composite film of Polyvinyl Alcohol-Expanded Graphite (PVA-EGr) as the positive triboelectric layer, Polyurethane (PU) as the negative triboelectric layer, and aluminum (Al) foil tape as electrodes. Various characterizations are performed to study the properties of the composite film and compared to pristine PVA film, including crystallographic structure, surface morphology, elemental composition, chemical bonding, and analysis of functional groups present in both films. Further, the electrical performance of the fabricated devices shows that the TENG with 0.4 g of EGr achieves the highest output voltage, current, and power of 264.68 V, 6.87 μA, and 2.88 mW, respectively. This optimized device demonstrates its capability by charging different capacitors and powering a series of green LEDs, highlighting its suitability for practical applications in electronic devices.

1 Introduction

Triboelectric nanogenerators (TENGs) have arisen as revolutionary devices with the ability to harness mechanical vibrations such as wind, ocean waves, and human motions and convert them into electrical power [1–3]. This functionality positions them as crucial components in the improvement of self-powered technologies, predominantly in portable and wearable electronics, sensors, and other low-power applications [4–6]. The fundamental principle of TENGs is based on triboelectrification and electrostatic induction where the charge transfer occurs when two differently charged materials come in contact and then separate, leading to a potential variance that drives the flow of charges, thereby generating an electric current [7–9]. The efficiency of TENGs significantly depends on factors such as the effective contact area, surface characteristics, surface engineering, and the electrical properties of the selected materials

Address correspondence to E-mail: sk@physics.uni-mysore.ac.in

https://doi.org/10.1007/s10854-025-14952-3

[10]. Materials with different electron affinities can boost charge transfer during contact and separation, thereby enhancing the output performance of TENG devices [11, 12]. The selection of materials for TENGs can be guided by the triboelectric series, which ranks materials based on their ability to gain or lose electrons [7]. Various polymers have demonstrated excellent triboelectric properties and have been widely used in the fabrication of TENG devices, including polydimethylsiloxane (PDMS), polyvinylidene difluoride (PVDF), polyvinyl alcohol (PVA), polypropylene (PP), polyvinyl chloride (PVC), and many more which are commonly used in TENGs, offer flexibility, ease of fabrication, and diverse triboelectric properties [13, 14]. Further addition of micro/nano additive materials with polymers enhances TENG performance by merging the beneficial characteristics of combination of materials, leading to more effective renovation of mechanical energy into electricity [15].

Among the traditional polymers utilized in TENG fabrication, PVA stands out as a commonly used synthetic polymer due to its desirable properties that enhance device performance. It possesses excellent film-forming ability and allows for the fabrication of uniform, flexible films, which is crucial for reliable TENG operation. The polymer's flexibility and mechanical strength make it suitable for applications requiring robust and adaptable materials, such as wearable and flexible electronics. Furthermore, PVA is biocompatible and non-toxic, making it ideal for biomedical applications where contact with human skin or tissues is necessary. PVA is cost-effective and widely available, contributing to the economic feasibility of large-scale TENG production [16–18]. Moreover, its hydrophilic nature facilitates surface modifications, allowing the tuning of triboelectric properties or better integration with other materials in the TENG structure [19]. Surface modification is a highly effective strategy for improving the performance of devices, achieved through both chemical and physical methods. Enhancing the contact area at the atomic scale on a polymer surface increases the number of contact points, thereby raising the surface charge density [20, 21]. Techniques such as mold imprinting micro/nano patterns [22], embedding nanoparticles or nanofillers, introducing porosity [23], plasma treatment [24], ion injection [25], and chemical modification [26] of the triboelectric layers have proven successful in boosting the efficiency of triboelectric nanogenerators (TENGs).

In this context, various nanofillers, including perovskites, carbon nanotubes (CNTs), MXenes, chalcogenides, ferroelectrics, metals, and metal oxides, are incorporated into polymer matrices due to their diverse electrical, dielectric, and surface properties [27–29]. Expanded Graphite (EGr) can also be one of the promising additives that have not been explored in the field of TENGs. EGr is a form of graphite that has experienced an expansion process through thermal exfoliation, resulting in a material with unique structural and functional characteristics [30, 31]. This expansion increases the spacing between layers, as intercalated compounds cause the layers to separate when heated, resulting in a worm-like structure and highly porous material [32, 33]. In addition, the process increases the surface area, flexibility, compressibility and electrical conductivity of EGr which is particularly beneficial for TENG fabrication [34–36]. Moreover, Egr's structural integrity and stability contribute to the durability of TENGs, making it appropriate for a wide array of applications [37].

In this study, a novel Polyvinyl Alcohol-Expanded Graphite-based TENG (PEGr-TENG) is developed using a PVA-EGr composite film as the positive triboelectric layer and a PU film as the negative triboelectric layer, where Al foil serves as the electrodes. Notably, this study marks the first integration of EGr being used in TENG fabrication. To evaluate the effect of varying EGr concentrations on the electrical performance of TENG, five distinct devices were fabricated, each incorporating different amounts of EGr in the PVA matrix (0.1, 0.2, 0.3, 0.4, and 0.5 g). The findings indicated that the TENG containing 0.4 g of EGr produced the maximum output voltage and current of 264.68 V and 6.87 μA, respectively. This optimized device was further utilized to demonstrate its practical applications, such as charging different capacitors and powering a series of 82 green light-emitting diodes (LEDs), highlighting its potential for advancing sustainable energy solutions.

2 Experimental section

2.1 Materials

PVA powder was received from Sigma Aldrich, USA. EGr was achieved from Sd fine-chem. Ltd., India. Commercial Al foil tape was employed for the assembly of the TENG devices. PU film was achieved

through solution casting method as detailed in our previous study [38].

2.2 PVA-EGr solution formation and TENG fabrication

The process for preparing PVA-EGr solution and fabricating the device is shown in Fig. 1a. For PVA, 100 mL of preheated (60 °C) deionized water was taken in a beaker and 7 g of PVA powder was added in the solution. A digital magnetic stirrer with 500 rpm was utilized to stir the mixture for 20 min, forming a 7% homogenous PVA solution. Then, EGr powder was incorporated to the PVA solution (maintaining the temperature at 60 °C) followed by an extra 10 min continuous stirring to achieve an even composite mixture. The composite solution was then dispensed into a petri dish and kept to dehydrated at normal ambient temperature for 2 days, forming a thin composite layer. The film was carefully removed and utilized for further characterization and device fabrication.

A portion of a polyethylene terephthalate (PET) bottle (6×10 cm^2) was utilized to structure the device, as detailed in our prior research [39]. Both the positive and negative triboelectric layers are cut into 4×4 cm^2 dimensions and attached onto the surface of Al foil tape and utilized as the top and bottom triboelectric layers of the TENG device, respectively (Fig. 1b). The layers are fixed to the internal surface of the polyethylene terephthalate (PET) bottle, creating an arch-shaped assembly. Figure 1c includes photographic images showcasing the frictional layers of the device with their dimension, and the arch structure with a 2 cm separation gap between layers. This design ensures

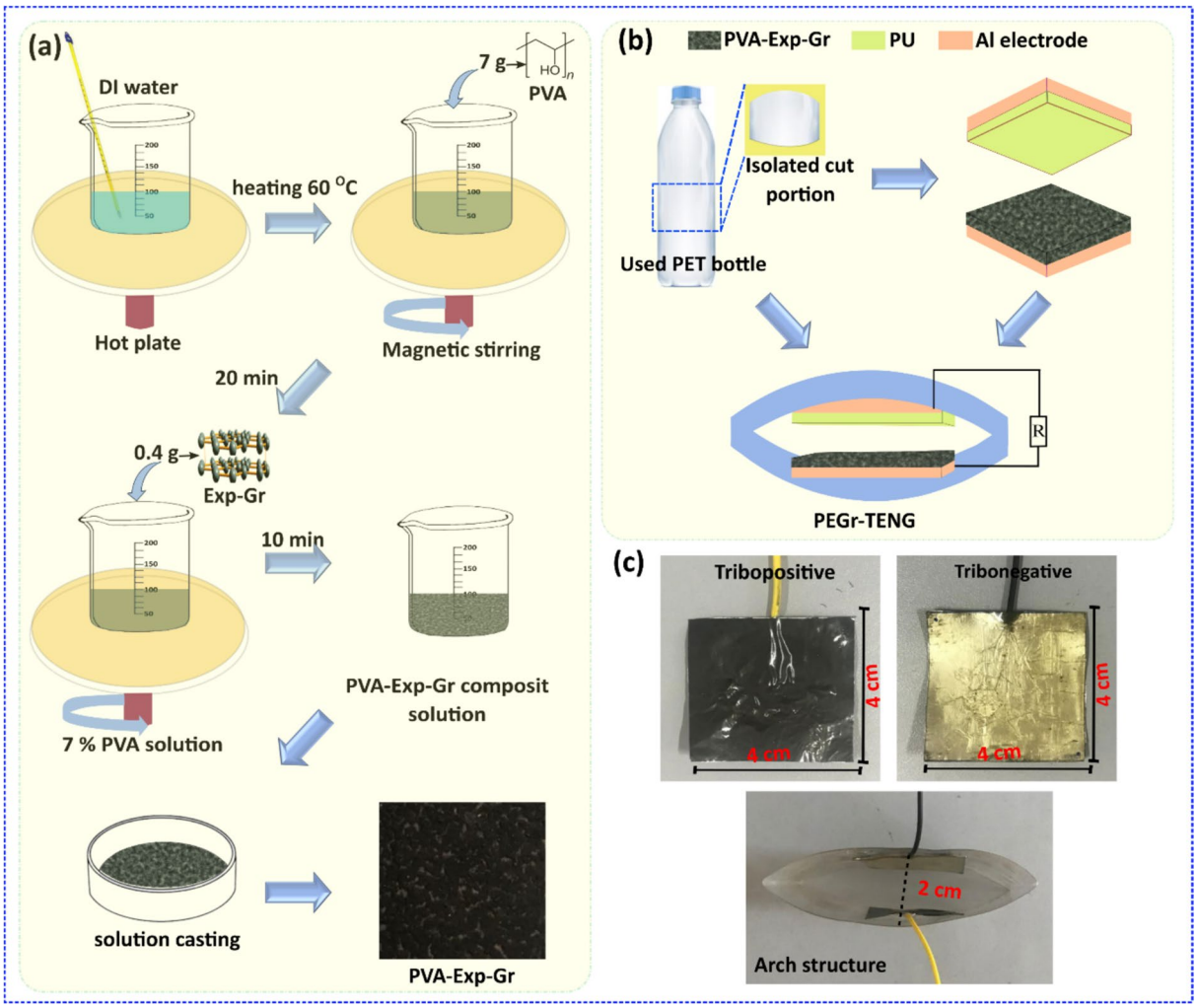

Fig. 1 **a** Schematic of composite solution formation and **b** TENG fabrication. **c** Photographic view of the assembled device

effective interaction between the triboelectric layers, enhancing the overall performance of the TENG device.

2.3 Characterizations

The phase determination and crystal structure of both PVA and PVA-EGr composite films were studied using Powder X-ray diffractometer (PXRD, PANALYTICAL, Netherlands) with a Cu Kα radiation source (λ = 0.1541 nm). Scanning electron microscopy tied with energy-dispersive X-ray spectroscopy (SEM with EDS, Zeiss EVOLS15, Germany) was employed to study the surface morphology and elemental composition of the prepared films. To investigate the interfacial interactions between PVA and EGr, Fourier transform infrared (FTIR) spectra was recorded using a Bruker OPUS 7.0 Alpha, covering a range from 400 to 4000 cm^{-1}. Further, a specially structured linear motor was utilized for generating continuous tapping energy for output performance of the device (Fig. S1 of the Supporting Information). Keithley source measure unit (model 2460, USA) was utilized for the electrical measurements of the PEGr-TENG.

3 Results and discussion

3.1 X-ray diffraction analysis

Powder X-ray diffraction (PXRD) is utilized to accomplish the structural analysis of the pristine PVA and PVA-EGr composite films. The PXRD profile of the pristine PVA film exhibits a broad and diffuse peak, appearing at around 19.5° corresponding to the (101) crystalline phase which indicates its semi-crystalline nature. In addition, a bulged peak at 21.8° is seen which corresponds to (200) amorphous phases of PVA [40]. The XRD analysis of PVA- graphite (Gr) and PVA-EGr composite films provides prominent structural differences between the two materials. For the PVA-Gr composite film, a discrete peak is detected at 26.7°, representing the typical (002) plane of Gr. This peak implies the layered structure of Gr, where the layers are closely stacked with a specific interlayer spacing, as discussed in a previous study [41]. However, in the PVA-EGr composite film, the distinct peak shifts to 25.4°, with a decrease in its intensity, suggesting an increased interlayer spacing between the Gr sheets. Further, the peak intensity reduction suggests a decline in crystallinity, indicating a less ordered structure with fewer stacked layers [42]. Furthermore, a small peak at 45.2° in the XRD pattern of PVA-EGr composites corresponds to the (100) plane of Gr (Fig. 2a). This peak is generally linked to the in-plane arrangement of carbon atoms within the Gr layers, reflecting the hexagonal lattice structure of Gr [43]. These observations confirm the successful expansion of Gr, resulting in exfoliated layers with larger inter layer spacing.

3.2 Surface morphological and elemental analysis

To study the surface morphology of pristine PVA and PVA-EGr composite films, Scanning electron microscopy (SEM) was employed. The SEM image of the pristine PVA film showcases a smooth surface, indicating its uniformity, as depicted in Fig. 2a. In contrast, the SEM image of the PVA-EGr composite film reveals a noticeably different texture, comparably a rougher surface with EGr particles evenly distributed throughout the PVA matrix. EGr has a high specific surface area due to its exfoliated structure, which provides a larger interfacial region when incorporated into the PVA matrix [44]. The increased roughness and expanded surface morphology facilitate a greater number of contact points between the frictional materials [45]. This enhancement in contact area directly contributes to improved triboelectric charge generation, as more surface interactions lead to greater charge accumulation during the contact-separation process of the TENG. EGr, being a carbon-based material with excellent electrical properties, plays a crucial role in enhancing charge trapping and retention in the triboelectric process. An optimum concentration of EGr in the PVA matrix increases the material's ability to hold triboelectric charges due to its larger interfacial region [46]. This improved charge storage capability leads to a higher surface charge density, ensuring efficient electron transfer during contact electrification [47]. However, an optimal concentration of EGr is necessary, as excessive loading may lead to conductivity-related charge dissipation, reducing the overall performance [48, 49].

Elemental analysis of both pristine PVA and PVA-EGr composite films was accomplished employing Energy Dispersive X-ray Spectroscopy (EDS). The EDS analysis inveterate the existence of Carbon (C) and Oxygen (O) in the pristine PVA film, verifying its

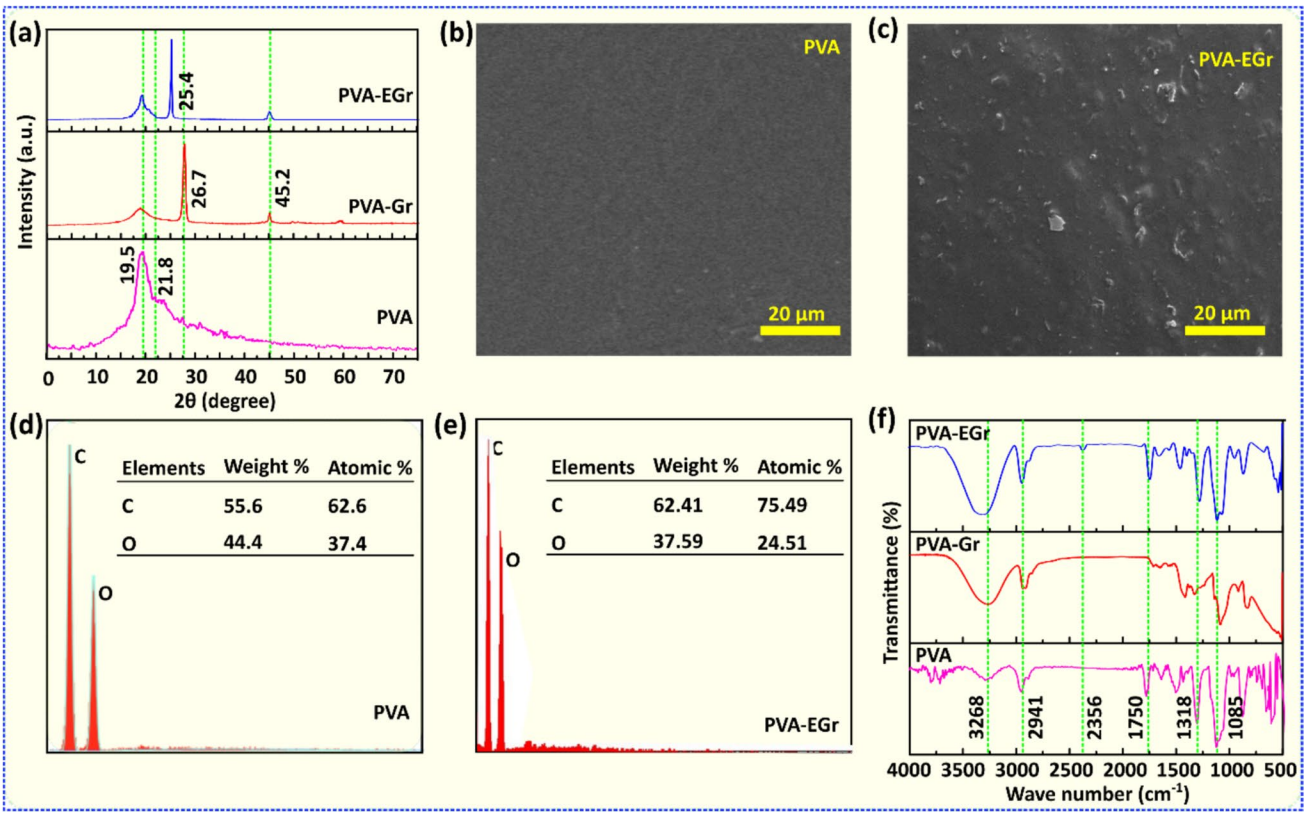

Fig. 2 **a** The XRD profile of PVA and PVA-EGr composite films. SEM image of **b** PVA and **c** PVA-EGr composite films. EDS spectrum of **d** pristine and **e** composite film. **f** FTIR spectra of both the films

purity (Fig. 2c). The elemental weight and atomic percentages are provided in the inset of Fig. 2c. Whereas, the EDS analysis of the PVA-EGr composite film shows an increased Carbon content, attributed to the addition of EGr (Fig. 2d). The corresponding elemental weight and atomic percentages are provided in the inset of Fig. 2d. This higher carbon concentration enhances the surface charge density of the film, resulting in improved charge transfer efficiency and better performance of the fabricated TENG [47].

3.3 Fourier transform infrared spectroscopic analysis

Fourier transform infrared spectroscopy (FTIR) is implemented to distinguish the functional groups present in a material and to understand the chemical interactions between different components. The FTIR spectra of both pristine PVA and the PVA-EGr composite film exhibit characteristic transmittance peaks at 1085 cm^{-1}, 1318 cm^{-1}, 1750 cm^{-1}, 2941 cm^{-1}, and 3268 cm^{-1}, equivalent to C–O stretching, C–H bending, C=O stretching, CH_2 stretching, and O–H stretching vibrations, respectively, which are typical of the PVA structure [50, 51]. Notably, a new peak appears at 2356 cm^{-1} in the PVA-EGr composite film, which is not present in the pristine PVA or standard Gr [52, 53]. The peak is due to the asymmetric stretching vibration of CO_2, indicates that the combination of EGr into the PVA matrix has led to the creation of new chemical interactions or bonds between the PVA polymer chains and EGr [54]. On the other hand, the increased peak intensity in the FTIR spectrum of PVA-EGr composite film, compared to that of the pristine PVA, showcases the successful integration of EGr into the PVA matrix [55]. Further, the increased intensity in FTIR spectrum implies a robust interaction among molecular components of the composite film which leads to an improved triboelectric property in TENG applications.

3.4 Working mechanism of PEGr-TENG

The PEGr-TENG operates in a vertical contact-separation method, utilizing the distinct properties of its components to generate energy. The device consists of triboelectric layers made from a PVA-EGr composite film and a PU film, supported by a PET substrate derived from a waste-water bottle. Al foil tape affixed to the back of each triboelectric layer serves as electrode. In the contact-separation mode, the device generates electricity through triboelectric effect and electrostatic induction processes [56]. Initially, when the PVA-EGr composite film and PU film come into contact by an external force, electrons transfer from the PU layer to the PVA-EGr layer due to their differing triboelectric properties. This electron transfer results in opposite charges accumulating on the surfaces of the two layers (Fig. 3a). As the applied force is reduced the layers detach from one another, a voltage difference (V) is generated between the electrodes due

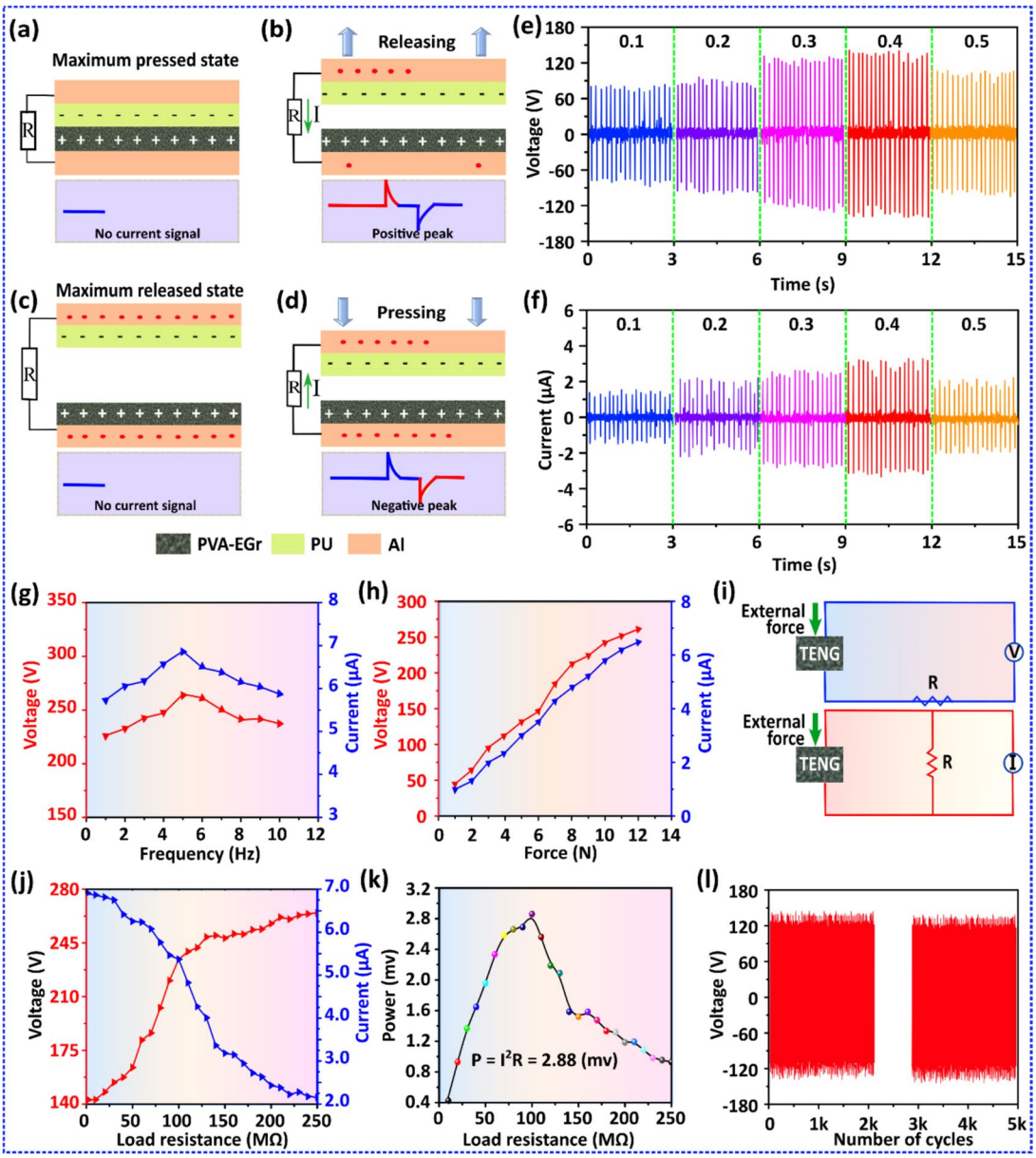

Fig. 3 **a–d** Working mechanism of PEGr-TENG. The generated **e** Voltage and **f** Current signals. **g** Effect of operation frequency and **h** force on output performance. **i** Circuit diagrams. **j** Output performance with respect to load resistance. **k** Generated power. **l** Stability test

to the separation of charges. This potential difference can be expressed by the formula $V = \sigma.d/\varepsilon_0$, where σ is the surface charge density, d is the distance between the triboelectric layers, and ε_0 is the permittivity of free space [57]. The electric field generated drives electrons through an external circuit from the electrode connected to the PVA-EGr layer to the electrode connected to the PU layer, generating an electric current (Fig. 3b). The charge flow drops to zero once when the triboelectric layers reach their extreme separation distance of 2 cm, as shown in Fig. 3c. Upon reapplication of the applied force, the layers come in contact, neutralizing the surface charges and causing the electrons to flow back over the external circuit in the opposite direction, producing another current pulse (Fig. 3d). This cyclic contact-separation process continuously generates alternating current (AC). The efficiency of power generation by TENG devices is directly affected by the surface charge density of the tribo layers, the interlayer separation distance, and the frequency of operation [58].

3.5 Electrical output performance and applications of PEGr-TENG

The electrical output performance of PEGr-TENG is studied using a custom structured linear motor to provide cyclic operations. To comprehend the influence of composite in electrical behavior of TENG devices, different devices were fabricated with varying EGr (0.1, 0.2, 0.3, 0.4, and 0.5 g) concentration in the PVA matrix. The devices were fabricated using the composite films as positive triboelectric and PU as negative triboelectric frictional layers with Al electrode. The devices with the dimensions 4×4 cm^2 operate in vertical contact separation mode for ease of fabrication and efficient operation. Figure 3e, f show the produced voltage and current signals, respectively, indicating that with increasing the composite concentration the output performance of TENG devices increases up to a certain value and then decreases. The increase in output performance is ascribed to the impact of EGr in PVA which enhances the effective surface contact area and boosts charge transfer efficiency of the device. The generated voltage and current by the devices are detailed in Table 1, indicating the device with an optimized composite concentration (0.4 g) of EGr generated the higher output voltage and current of 264.68 V and 6.87 μ A, respectively. The optimal performance at 0.4 g EGr is due to the balance between enhanced surface charge density and minimal charge dissipation. At this concentration, EGr improves conductivity and charge trapping without forming excessive conductive pathways [59, 60]. However, at 0.5 g EGr, the increased conductivity creates percolation networks, leading to charge leakage and reduced triboelectric output [61].

Table 1 The electrical output performance of PEGr-TENGs

Frictional layers		Electrode	Electrical output performance	
Bottom	Top		Voltage (V)	Current (μA)
PVA-EGr 0.1	PU	Al	164.23	3.41
PVA-EGr 0.2			180.54	4.38
PVA-EGr 0.3			248.31	5.39
PVA-EGr 0.4			**264.68**	**6.87**
PVA-EGr 0.5			228.81	4.13

Bold values indicate optimized device output (PVA-EGr 0.4g) in comparison to other devices

The increase in composite concentration beyond this optimized level reduces the overall performance of TENG devices due to the agglomeration of EGr nanosized particles in the composite film. In addition, the device's output was measured using four different tribonegative layers including polyethylene terephthalate (PET), fluorinated ethylene propylene (FEP), polylactic acid (PLA), and polyvinylidene fluoride (PVDF). The recorded output voltage and current for each layer were as follows: 94.12 V / 2.35 μA (PET), 125.34 V/3.28 μA (FEP), 175.81 V/3.69 μA (PLA), and 214.62 V/4.43 μA (PVDF). These results demonstrate that the PEGr-TENG achieves comparatively higher output when paired with a PU layer. The corresponding voltage and current signals are presented in Fig S2 of the Supporting Information. Furthermore, the mechanical durability and electrical stability of the devices were evaluated over 5000 operational cycles, showing stable output performance across all variations, confirming their reliability (Fig S3, Supporting Information). Additionally, the energy conversion efficiency was calculated for each TENG configuration: 2.7% (PET-TENG), 6.2% (FEP-TENG), 9.4% (PLA-TENG), 17.7% (PVDF-TENG), and 20.9% (PEGr-TENG). Detailed calculation methods are provided in Note S1 of the Supporting Information. Therefore, the optimized device is utilized for further characterizations and applications.

The generated output of the optimized PEGr-TENG device was studied under varying applied frequencies ranging from 2 to 12 Hz. The output performance increased with increasing frequency up to 5 Hz, resembling the resonance frequency of the device, and then reduced due to the rapid cyclic operation avoiding the layers from attaining their supreme inter layer separation distance (Fig. 3g) [62]. Additionally, the output performance was examined with changing applied forces ranging from 2 to 12 N. Figure 3h indicates that generated voltage and current by the device increased with cumulative applied force, demonstrating the device's capability to convert more mechanical energy efficiently. Furthermore, the device's output voltage and current were analyzed under different load resistances. The circuit diagram for measuring voltage and current is illustrated in Fig. 3i (top and bottom, respectively). Figure 3j shows that with increasing resistance, the produced voltage of the device improved while the current declined, satisfying Ohm's law [63]. The point at which both the voltage and current curves meet each other corresponds to the optimal load resistance of the TENG, at which the device generates the maximum power. The generated power by the device was calculated using the formula $P = I^2R$,, where I is the instantaneous current and R is the load resistance. The device achieved a peak power output of 2.88 mW, which can be used for operating small-scale electronic devices (Fig. 3k). Finally, the device's electrical stability was evaluated by subjecting it to 5000 continuous operational cycles. The generated voltage signals, presented in Fig. 3l, demonstrate consistent electrical output throughout the test, indicating the mechanical robustness and electrical reliability of the fabricated TENG device.

4 Applications of PEGr-TENG

TENGs typically convert mechanical vibrations into electrical power, generating AC current, which is unsuitable for powering most electronics that use direct current (DC). To address this limitation, a rectifier is crucial for converting the AC output of the TENG into usable DC power. The PEGr-TENG was employed to charge electrolytic capacitors, demonstrating its potential for practical energy storage applications. The circuit diagram in Fig. 4a illustrates the device's connection to a rectifier bridge. The device successfully charged three electrolytic capacitors with capacitances of 2.2, 3.3, and 4.7 μF to voltages of 6.7, 5.02, and 2.97 V, respectively, as shown in Fig. 4b. This process demonstrates the PEGr-TENG's versatility in accommodating various capacitor sizes and

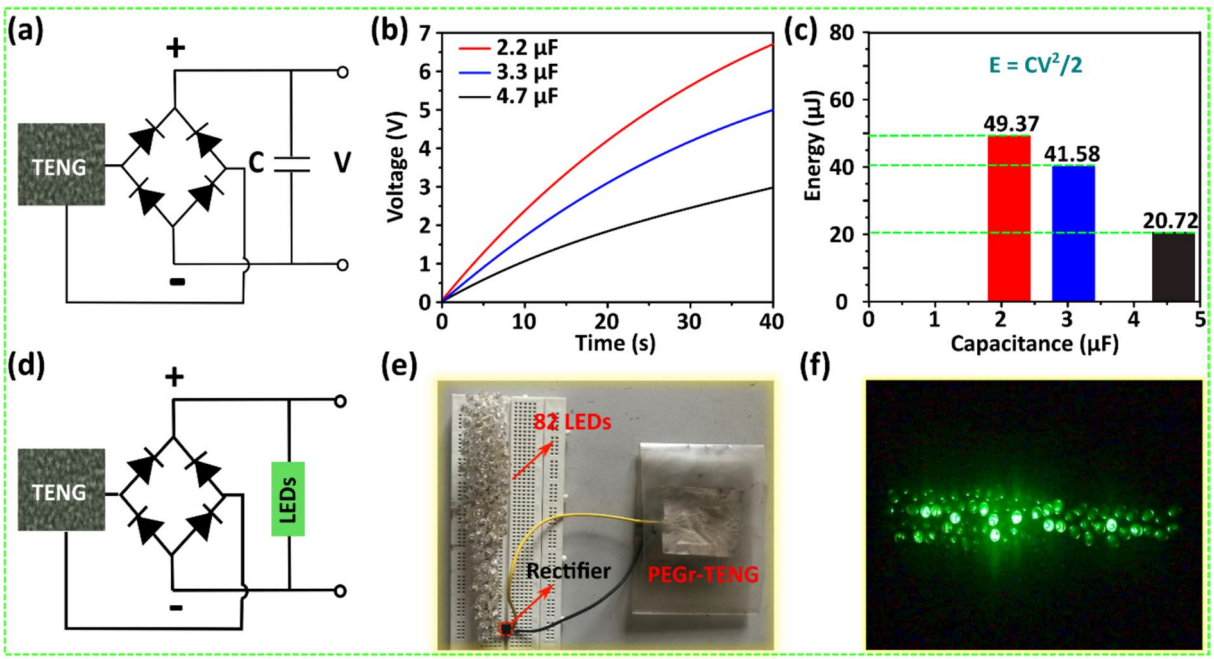

Fig. 4 **a** Schematic circuit illustration and **b** charging curves for the capacitors. **c** Energy stowed in the capacitors. **d** Circuit connection for glowing LEDs. **e** The photographic representation of the device with LEDs. **f**) Powering LEDs

its effectiveness in energy storage. The energy stored in each capacitor was calculated using the formula $E = 1/2CV^2$, where C is the capacitance and V is the corresponding voltage. The calculated energy values were 49.37 μJ for the 2.2 μF capacitor, 41.58 μJ for the 3.3 μF capacitor, and 20.72 μJ for the 4.7 μF capacitor. Figure 4c shows that the 2.2 μF capacitor stored the most electrical energy, making it suitable for powering small-scale electronic devices. The efficient energy storage in the capacitors demonstrates the TENG's potential for use in various applications that require reliable and portable power sources. Further, the device demonstrated its practical application by successfully lighting up a series of green LEDs (Video S1, Supporting Information).

The circuit diagram for powering the LEDs is provided in schematic Fig. 4d, illustrating the setup required to connect the TENG to the series of green LEDs. A photographic image in Fig. 4e displays the device connectivity with the rectifier bridge and LEDs. Figure 4f shows the powering of 82 green LEDs by the PEGr-TENG using hand tapping energy. This demonstration underscores the device's effectiveness and potential for practical applications in real-world scenarios, showcasing its capability to convert mechanical energy into electrical energy efficiently. Further, the scalability of the EGr TENG is promising due to the use of low-cost, commercially available materials and simple fabrication techniques. PVA-EGr, PU, and Al foil tape are widely accessible, making large-scale production feasible. For industrial applications, key considerations include the uniform dispersion of EGr in PVA, ensuring consistent triboelectric performance across large-area devices. Optimizing the fabrication process, such as using automated coating techniques and scalable drying methods, would enhance reproducibility and efficiency. Moreover, integrating flexible and stretchable substrates could improve the mechanical durability of the device, making it more suitable for wearable and structural energy-harvesting applications.

5 Conclusion

In this study, a novel PEGr-TENG was successfully fabricated, for the first time, using a PVA-EGr composite film as the positive triboelectric layer and PU film as the negative triboelectric layer, with Al serving as electrodes. The XRD analysis confirmed the successful expansion of graphite in the PVA-EGr composite, evidenced by the shift in the diffraction peak and reduced crystallinity. SEM and EDS were employed to analyze the surface structure and elemental composition of both pristine PVA and PVA-EGr composite films. SEM images exhibited a smooth surface for the pristine PVA film, while the PVA-EGr composite film revealed a rougher texture with a uniform dispersion of EGr particles. EDS analysis confirmed the purity of the pristine PVA film and highlighted a higher carbon content in the PVA-EGr composite, which contributes to improved charge transfer efficiency. In addition, FTIR showed both familiar and new peaks in the composite film, signifying improved chemical interactions and more robust bonding between the PVA and EGr components. These structural and chemical changes improve the triboelectric performance of the material in TENG applications. The impact of EGr in electrical output of TENG was investigated. Whereas, the device with 0.4 g of EGr generated the highest output voltage, current, and power of 264.68 V, 6.87 μA, and 2.88 mW, respectively. The optimized device successfully charged various electrolytic capacitors and powered 82 green LEDs using manual tapping. This study illustrates the PEGr-TENG's capability to deliver reliable and portable power, advancing the development of sustainable and intelligent energy solutions.

Author contributions

Sebghatullah Amini: Conceptualization, Data curation, Formal analysis, Investigation, Methodology, Validation, Writing—review & editing. Rumana Farheen S. M. A.: Conceptualization, Data curation, Validation, Writing—original draft, review & editing. Sangamesha M. A.: Methodology, Visualization, and resources. Krishnaveni Sannathammegowda: Supervision, Validation, and Visualization.

Funding

Sebghatullah Amini is financially supported by the Indian Council for Cultural Relations (ICCR) scholarship, the government of India. Rumana Farheen S.M. acknowledges the Council of Scientific and Industrial Research (CSIR), Government of India, for the financial assistance provided under the Research Associate fellowship (File no. 364-4194-9498/2K23/1).

Data availability

Data will be made available on request.

Declarations

Competing interest The authors declare that they have no known competing financial interests or personal relationships that could have appeared to influence the work reported in this paper.

Supplementary Information The online version contains supplementary material available at https://doi.org/10.1007/s10854-025-14952-3.

References

1. W. Kim, D. Kim, I. Tcho, J. Kim, M. Kim, Y. Choi, Triboelectr. Nanogenerator Struct. Mech. Appl. (2021). https://doi.org/10.1021/acsnano.0c09803
2. V.L. Yashaswini, S.M.R. Farheen, B.P. Mahadevaswamy, B.S. Madhukar, M.A. Sangamesha, S. Krishnaveni, Synergistic effects of rGO functionalization in nanocomposite-based triboelectric nanogenerators for enhanced energy harvesting. Sens. Actuators A Phys. **370**, 115200 (2024)
3. S. Amini, R.F.S.M. Ahmed, S. Kumar, S.M. Ankanathappa, K. Sannathammegowda, Electrifying waste textiles: Transforming fabric scraps into high-performance triboelectric nanogenerators for biomechanical energy harvesting. Waste Manag. **190**, 477–485 (2024)
4. V. Vivekananthan, A. Chandrasekhar, N.R. Alluri, Y. Purusothaman, G. Khandelwal, S.-J. Kim, Triboelectric nanogenerators: design, fabrication, energy harvesting, and portable-wearable applications. Nanogenerators **5**, 3 (2020)
5. J. Luo, Z.L. Wang, Recent progress of triboelectric nanogenerators: From fundamental theory to practical applications. EcoMat. **2**, e12059 (2020)
6. S. Amini, R.F. Sagade Muktar Ahmed, S. Madanahalli Ankanathappa, K. Sannathammegowda, Polyaniline-doped textile-based triboelectric nanogenerator: self-powered device for wearable electronics. Appl. Res. **4**, e202400124 (2024)
7. P. Maharjan, T. Bhatta, C. Park, H. Cho, K. Shrestha, S. Lee, M. Salauddin, M.T. Rahman, S.S. Rana, J.Y. Park, High-performance keyboard typing motion driven hybrid nanogenerator. Nano Energy **88**, 106232 (2021). https://doi.org/10.1016/j.nanoen.2021.106232
8. K. Wang, Y. Weng, G. Chen, C. Wu, J.H. Park, Z. Qiu, J. Wang, Y. Liu, Y. Zhang, X. Zhou, Coupling electrostatic induction and global electron circulation for constant-current triboelectric nanogenerators. Nano Energy **85**, 105929 (2021)
9. T.K. Nanditha, S. Bhat, S. Amini, S.M. Rumana Farheen, R. Waiker, R.G. Sonkawade, M.A. Sangamesha, M. Ballal, S. Krishnaveni, S.C. Gurumurthy, Robust Ag–Co bimetallic nanoparticles: dual role in catalytic and triboelectric performance. Mater. Res. Bull. **180**, 113061 (2024)
10. S.A. Lone, K.C. Lim, K. Kaswan, S. Chatterjee, K.-P. Fan, D. Choi, S. Lee, H. Zhang, J. Cheng, Z.-H. Lin, Recent advancements for improving the performance of triboelectric nanogenerator devices. Nano Energy. **99**, 107318 (2022)
11. K. Shi, B. Chai, H. Zou, Z. Wen, M. He, J. Chen, P. Jiang, X. Huang, Contact electrification at adhesive interface: boosting charge transfer for high-performance triboelectric nanogenerators. Adv. Funct. Mater. **33**, 2307678 (2023)
12. C.M. Veerabhadraswamy, S.N. Rashmi, S.M. MizbaTazleem, S. Puneeth, S.M. Rumana Farheen, M.A. Sangamesha, S. Krishnaveni, Novel approach to bio-inspired triboelectric nanogenerators employing recycled natural fibres for sustainable energy harvesting. Sens. Actuators A Phys. **377**, 115678 (2024)
13. B. Dudem, N.D. Huynh, W. Kim, D.H. Kim, H.J. Hwang, D. Choi, J.S. Yu, Nanopillar-array architectured PDMS-based triboelectric nanogenerator integrated with a windmill model for effective wind energy harvesting. Nano Energy **42**, 269–281 (2017)
14. R.F.S.M. Ahmed, S. Amini, R. Gopalakrishnan, S.M. Ankanathappa, K. Sannathammegowda, Copper selenide as a facile nanomaterial for triboelectric nanogenerator: Self-powered Braille code keyboard. Chem. Eng. J. **500**, 156706 (2024)
15. J.P. Hou, R. Li, Q. Wang, H.Y. Yu, Z.J. Zhang, Q.Y. Chen, H. Ma, X.M. Wu, X.W. Li, Z.F. Zhang, Three principles for preparing Al wire with high strength and high electrical conductivity. J. Mater. Sci. Technol. **35**, 742–751 (2019)
16. Q. Xu, Z. Wu, W. Zhao, M. He, N. Guo, L. Weng, Z. Lin, M.F.A. Taleb, M.M. Ibrahim, M.V. Singh, Strategies in the preparation of conductive polyvinyl alcohol hydrogels for applications in flexible strain sensors, flexible supercapacitors, and triboelectric nanogenerator sensors: an overview. Adv. Compos. Hybrid Mater. **6**, 203 (2023)
17. I.J. Chung, W. Kim, W. Jang, H.-W. Park, A. Sohn, K.-B. Chung, D.-W. Kim, D. Choi, Y.T. Park, Layer-by-layer assembled graphene multilayers on multidimensional surfaces for highly durable, scalable, and wearable

triboelectric nanogenerators. J. Mater. Chem. A. **6**, 3108–3115 (2018)
18. Q. Wang, B. Xu, D. Tan, X. Hu, Y. Yang, J. Huang, Y. Gao, X. Liu, Nature-inspired scalable high-performance triboelectric nanogenerators for energy harvesting and sensing. Nano Energy **121**, 109217 (2024)
19. X. Sun, L. Dong, Y. Liu, X. Li, J. Liu, N. Wang, Y. Liu, X. Li, D. Wang, S. Chen, Biomimetic PVA-PVDF-based triboelectric nanogenerator with MXene doping for self-powered water sterilization. Mater. Today Nano. **24**, 100410 (2023)
20. G. Hurwitz, G.R. Guillen, E.M.V. Hoek, Probing polyamide membrane surface charge, zeta potential, wettability, and hydrophilicity with contact angle measurements. J. Memb. Sci. **349**, 349–357 (2010)
21. J. Wu, X. Wang, H. Li, F. Wang, W. Yang, Y. Hu, Insights into the mechanism of metal-polymer contact electrification for triboelectric nanogenerator via first-principles investigations. Nano Energy **48**, 607–616 (2018)
22. S. Cho, S. Jang, M. La, Y. Yun, T. Yu, S.J. Park, D. Choi, Facile tailoring of contact layer characteristics of the triboelectric nanogenerator based on portable imprinting device. Materials (Basel) **13**, 872 (2020). https://doi.org/10.3390/ma13040872
23. M.M. Rastegardoost, O.A. Tafreshi, Z. Saadatnia, S. Ghaffari-Mosanenzadeh, C.B. Park, H.E. Naguib, Recent advances on porous materials and structures for high-performance triboelectric nanogenerators. Nano Energy **111**, 108365 (2023)
24. G.-G. Cheng, S.-Y. Jiang, K. Li, Z.-Q. Zhang, Y. Wang, N.-Y. Yuan, J.-N. Ding, W. Zhang, Effect of argon plasma treatment on the output performance of triboelectric nanogenerator. Appl. Surf. Sci. **412**, 350–356 (2017)
25. J. Seo, S. Hajra, M. Sahu, H.J. Kim, Effect of cilia microstructure and ion injection upon single-electrode triboelectric nanogenerator for effective energy harvesting. Mater. Lett. **304**, 130674 (2021)
26. Y. Nurmakanov, G. Kalimuldina, G. Nauryzbayev, D. Adair, Z. Bakenov, Structural and chemical modifications towards high-performance of triboelectric nanogenerators. Nanoscale Res. Lett. **16**, 122 (2021)
27. H. Wang, M. Shi, K. Zhu, Z. Su, X. Cheng, Y. Song, X. Chen, Z. Liao, M. Zhang, H. Zhang, High performance triboelectric nanogenerators with aligned carbon nanotubes. Nanoscale **8**, 18489–18494 (2016)
28. C.C. Gowda, R. Tromer, D. Chandravanshi, P. Pandey, K. Chattopadhyay, D.S. Galvao, C.S. Tiwary, Two-dimensional manganese di-telluride based triboelectric nanogenerator. Nano Energy **117**, 108833 (2023)
29. X. Suo, B. Li, H. Ji, S. Mei, S. Miao, M. Gu, Y. Yang, D. Jiang, S. Cui, L. Chen, Dielectric layer doping for enhanced triboelectric nanogenerators. Nano Energy **114**, 108651 (2023)
30. G. Zheng, J. Wu, W. Wang, C. Pan, Characterizations of expanded graphite/polymer composites prepared by in situ polymerization. Carbon N. Y. **42**, 2839–2847 (2004)
31. Y. Wen, K. He, Y. Zhu, F. Han, Y. Xu, I. Matsuda, Y. Ishii, J. Cumings, C. Wang, Expanded graphite as superior anode for sodium-ion batteries. Nat. Commun. **5**, 4033 (2014)
32. A.V. Yakovlev, A.I. Finaenov, S.L. Zabud'Kov, E.V. Yakovleva, Thermally expanded graphite: synthesis, properties, and prospects for use. Russ. J. Appl. Chem. **79**, 1741–1751 (2006)
33. A.G. Olabi, T. Wilberforce, K. Elsaid, E.T. Sayed, M. Ramadan, S.M.A. Rahman, M.A. Abdelkareem, Recent progress on carbon-based nanomaterial for phase change materials: prospects and challenges. Therm. Sci. Eng. Prog. **23**, 100920 (2021)
34. N. Saadat, H.N. Dhakal, J. Tjong, S. Jaffer, W. Yang, M. Sain, Recent advances and future perspectives of carbon materials for fuel cell. Renew. Sustain. Energy Rev. **138**, 110535 (2021)
35. J. Shi, M. Qin, W. Aftab, R. Zou, Flexible phase change materials for thermal energy storage. Energy Storage Mater. **41**, 321–342 (2021)
36. Y.F. Zhao, M. Xiao, S.J. Wang, X.C. Ge, Y.Z. Meng, Preparation and properties of electrically conductive PPS/expanded graphite nanocomposites. Compos. Sci. Technol. **67**, 2528–2534 (2007)
37. D. Tantraviwat, M. Ngamyingyoud, W. Sripumkhai, P. Pattamang, G. Rujijanagul, B. Inceesungvorn, Tuning the dielectric constant and surface engineering of a BaTiO3/Porous PDMS composite film for enhanced triboelectric nanogenerator output performance. ACS Omega **6**, 29765–29773 (2021)
38. R.F.S.M. Ahmed, S.K.K. Swamy, G.S. Chandrasekhar, S.M. Ankanathappa, A. Chandrasekhar, K. Sannathammegowda, *Clitoria Ternatea* flower extract: biopolymer composite-based triboelectric nanogenerator as a self-powered smart counter. Surf. Interfaces. **42**, 103369 (2023)
39. R.F.S.M. Ahmed, S. Amini, S.M. Ankanathappa, K. Sannathammegowda, Electricity out of electronic trash: triboelectric nanogenerators from discarded smartphone displays for biomechanical energy harvesting. Waste Manag. **178**, 1–11 (2024)
40. R. Kouser, A. Vashist, M. Zafaryab, M.A. Rizvi, S. Ahmad, pH-responsive biocompatible nanocomposite hydrogels for therapeutic drug delivery. ACS Appl. Bio Mater. **1**, 1810–1822 (2018)

41. S. Amini, R.F.S.M. Ahmed, S.M. Ankanathappa, M.H.C. Shastry, M. Shivanna, K. Sannathammegowda, Investigating the annealing effects on the performance of polyvinyl alcohol-graphite-based triboelectric nanogenerator. Sens. Actuators A Phys. **372**, 115309 (2024)
42. L.-Z. Bai, D.-L. Zhao, T.-M. Zhang, W.-G. Xie, J.-M. Zhang, Z.-M. Shen, A comparative study of electrochemical performance of graphene sheets, expanded graphite and natural graphite as anode materials for lithium-ion batteries. Electrochim. Acta **107**, 555–561 (2013)
43. L. Huang, S.-R. Chen, S.-L. Chou, S.X. Dou, Facile synthesis of a interleaved expanded graphite-embedded sulphur nanocomposite as cathode of Li–S batteries. J. Mater. Chem. **22**, 4744–4750 (2012)
44. J. Orellana, E. Araya-Hermosilla, A. Pucci, R. Araya-Hermosilla, Polymer-assisted graphite exfoliation: advancing nanostructure preparation and multifunctional composites. Polymers (Basel) **16**, 2273 (2024)
45. A. Ahmed, I. Hassan, A.M. Pourrahimi, A.S. Helal, M.F. El-Kady, H. Khassaf, R.B. Kaner, Toward high-performance triboelectric nanogenerators by engineering interfaces at the nanoscale: looking into the future research roadmap. Adv. Mater. Technol. **5**, 2000520 (2020)
46. G. Prasad, J.U. Yoon, I. Woo, J.W. Bae, Fabrication of amino and fluorine functionalized graphene-based polymer composites to enhance the electromechanical conversion efficiency of TENGs for energy-harvesting applications. Chem. Eng. J. **470**, 144280 (2023)
47. Y. Liu, J. Mo, Q. Fu, Y. Lu, N. Zhang, S. Wang, S. Nie, Enhancement of triboelectric charge density by chemical functionalization. Adv. Funct. Mater. **30**, 1–33 (2020). https://doi.org/10.1002/adfm.202004714
48. K. Xiao, W. Wang, K. Wang, H. Zhang, S. Dong, J. Li, Improving triboelectric nanogenerators performance via interface tribological optimization: a review. Adv. Funct. Mater. (2024). https://doi.org/10.1002/adfm.202404744
49. J. Wang, H. Wu, S. Fu, G. Li, C. Shan, W. He, C. Hu, Enhancement of output charge density of TENG in high humidity by water molecules induced self-polarization effect on dielectric polymers. Nano Energy **104**, 107916 (2022)
50. M.M. Atta, E.O. Taha, A.M. Abdelreheem, Nitrogen plasma effect on the structural, thermal, and dynamic mechanical properties of PVA/starch/graphene oxide nanocomposite. Appl. Phys. A **127**, 532 (2021)
51. N. Subramanian, N. Sundaraganesan, S. Sudha, V. Aroulmoji, G.D. Sockalingam, M. Bergamin, Experimental and theoretical investigation of the molecular and electronic structure of anticancer drug camptothecin. Spectrochim. Acta Part A Mol. Biomol. Spectrosc. **78**, 1058–1067 (2011)
52. H. Zhao, R. Lin, Preparation of boric acid modified expandable graphite and its influence on polyethylene combustion characteristics. J. Chil. Chem. Soc. **61**, 2767–2771 (2016)
53. J.R. Kim, S. Michielsen, Photodynamic antifungal activities of nanostructured fabrics grafted with rose bengal and phloxine B against A spergillus fumigatus. J. Appl. Polym. Sci. (2015). https://doi.org/10.1002/app.42114
54. Z.M. El-Bahy, A.I. Hanafy, M.M. Ibrahim, M. Anpo, In situ FTIR studies of CO oxidation over Fe-free and Fe-promoted PtY catalysts: effect of water vapor addition. J. Mol. Catal. A Chem. **344**, 111–121 (2011)
55. O.A. Adeniran, Role of engine age and lubricant chemistry on the characteristics of EGR soot, (2014).
56. Z.L. Wang, L. Lin, J. Chen, S. Niu, Y. Zi, Z.L. Wang, L. Lin, J. Chen, S. Niu, Y. Zi, *Triboelectric nanogenerator: Vertical contact-separation mode, triboelectric nanogenerators* (Springer, Cham, 2016), pp.23–47
57. Z. Zhang, N. Yin, Z. Wu, S. Pan, D. Wang, Research methods of contact electrification: theoretical simulation and experiment. Nano Energy **79**, 105501 (2021)
58. Z. Lin, J. Chen, J. Yang, Recent progress in triboelectric nanogenerators as a renewable and sustainable power source. J. Nanomater. **2016**, 5651613 (2016)
59. C. Wang, H. Guo, P. Wang, J. Li, Y. Sun, D. Zhang, An advanced strategy to enhance TENG output: reducing triboelectric charge decay. Adv. Mater. **35**, 2209895 (2023)
60. C.K. Ao, Y. Jiang, L. Zhang, C. Yan, J. Ma, C. Liu, Y. Jiang, W. Zhang, S. Soh, Balancing charge dissipation and generation: mechanisms and strategies for achieving steady-state charge of contact electrification at interfaces of matter. J. Mater. Chem. A. **10**, 19572–19605 (2022)
61. Y. Li, Y. Luo, H. Deng, S. Shi, S. Tian, H. Wu, J. Tang, C. Zhang, X. Zhang, J. Zha, Advanced dielectric materials for triboelectric nanogenerators: principles, methods, and applications. Adv. Mater. (2024). https://doi.org/10.1002/adma.202314380
62. C. Wu, R. Liu, J. Wang, Y. Zi, L. Lin, Z.L. Wang, A spring-based resonance coupling for hugely enhancing the performance of triboelectric nanogenerators for harvesting low-frequency vibration energy. Nano Energy **32**, 287–293 (2017)
63. H. Zhou, G. Liu, J. Zeng, Y. Dai, W. Zhou, C. Xiao, T. Dang, W. Yu, Y. Chen, C. Zhang, Recent progress of switching power management for triboelectric nanogenerators. Sensors **22**, 1668 (2022)